**Atmospheric
Chemistry
and Physics
Discussions**

AMALi – the Airborne Mobile Aerosol Lidar for Arctic research

I. S. Stachlewska[1,2]**, R. Neuber**[1]**, A. Lampert**[1]**, C. Ritter**[1]**, and G. Wehrle**[1,3]

[1]Alfred Wegener Institute for Polar and Marine Research, Telegrafenberg A43,
14473 Potsdam, Germany
[2]Institute of Geophysics, Faculty of Physics, University of Warsaw, Pasteura 7,
02-093 Warsaw, Poland
[3]Laboratory of Atmospheric Chemistry, Paul Scherrer Institut, 5232 Villigen PSI, Switzerland

ACPD

9, 18745–18792, 2009

AMALi

I. S. Stachlewska et al.

Title Page

Abstract	Introduction
Conclusions	References
Tables	Figures

| ◄◄ | ►► |
| ◄ | ► |

| Back | Close |

Full Screen / Esc

Printer-friendly Version

Interactive Discussion

Abstract

The Airborne Mobile Aerosol Lidar (AMALi) is an instrument developed at the Alfred Wegener Institute for Polar and Marine Research for a trouble-free operation under the challenging weather conditions at the Earth's polar regions. Since 2003 the AMALi has been successfully deployed for measurements in the ground-based installation and the zenith- or nadir-aiming airborne configurations during several scientific campaigns in the Arctic. The lidar provides profiles of the total backscatter at two wavelengths, from which aerosol and cloud properties are derived. It measures also the linear depolarization of the backscattered return, allowing for the discrimination of thermodynamic cloud phase and the identification of the presence of non-spherical aerosol particles. This paper presents the capability characteristics and performance of the past and present state of the AMALi system, as well as discusses the ground-based and airborne evaluation schemes applied to invert the data.

1 Introduction

One of the primary objectives of the Atmospheric Division at the Alfred Wegener Institute for Polar and Marine Research (AWI), Research Unit Potsdam, is to improve the understanding of the direct and indirect effects of Arctic aerosol as well as clouds on the climate system. The full assessment can be accomplished only by collaborative studies of Arctic aerosol-cloud-climate interactions by combining the experimental data of aerosol and cloud properties obtained from local observatories, field campaigns, and satellite measurements (Treffeisen et al., 2004; Yamanouchi et al., 2005) applied together with a sophisticated regional climate model, especially designed for the Arctic (Dethloff et al., 1996; Rinke et al., 2004).

The main focus of the Lidar Group at the AWI Potsdam Research Unit is to provide the observations of Arctic aerosol and clouds necessary for the modeling activities, and investigate the properties of the Arctic atmosphere via designing, building and

Full Screen / Esc

operating lidar systems suitable for measurements in difficult Arctic conditions. The Airborne Mobile Aerosol Lidar (AMALi) was developed in 2003 by the AWI Potsdam Lidar Group (Stachlewska et al., 2004) and has been successfully serving, integrated on board the AWI's Polar 2, a Do-228 research aircraft, during several international campaigns. Since 2009, the AMALi is also certified for operation on board the AWI's Polar 5, a Basler BT-67 research aircraft.

In 2006, the AMALi system was modified. The change of the detection wavelengths from the first and the second Nd:YAG harmonics (1064 nm and 532 nm) to the second and third harmonics (532 nm and 355 nm) promised an improved capability for detecting the small Arctic Haze aerosol particles. Due to the possibility of operating the AMALi system in a zenith-aiming configuration with an extended range (opening on the roof), the option of reading out the signals in both analog and photon counting mode was included.

Data obtained from zenith-aiming airborne measurements can be used for the validation of vertical profiles of aerosol and cloud backscatter and depolarization of the Cloud-Aerosol LIdar with Orthogonal Polarization (CALIOP) on board of the Cloud-Aerosol Lidar and Infrared Pathfinder Satellite (CALIPSO; Winker et al., 2007). Furthermore, it is possible to investigate aerosol layers in the free troposphere as well as midlevel and high cirrus clouds for flights at low altitude.

Before the Arctic campaigns took place, the system was validated and tested during January–April 2004 and August–December 2006 by performing ground based investigations of the diurnal boundary layer cycle from the AWI's Lidar Laboratory in Potsdam. Additionally, robust construction and trouble-free operation of the AMALi was proved during the lidar test flights in April 2004, March 2005 and July 2006. This allowed for an airborne investigation of the sea-land aerosol gradients over the north-western coastline offshore Bremerhaven.

The lidar group performed high quality airborne observations of various atmospheric events with the AMALi system operated in nadir-aiming configuration during the Arctic Study of Aerosol, Clouds and Radiation ASTAR 2004 and the Svalbard Experiment

SVALEX 2005 campaigns in the Arctic. After the modification, the AMALi was operated in alternatively nadir or zenith configuration during the ASTAR 2007 and Pan-Arctic Measurements Arctic Regional Climate Model Intercomparison PAM-ARCMIP 2009 campaigns.

The campaigns resulted in several case studies involving the AMALi:

– investigations of clean versus polluted Arctic conditions (Stachlewska et al., 2005),

– characteristics of the lidar ratio profiles over Ny-Ålesund obtained from the two-stream and the Raman lidar data evaluation methods (Stachlewska and Ritter, 2009),

– marine boundary layer observations offshore Svalbard and their interpretation with the ECMWF (Stachlewska and Dörnbrack, 2006a),

– extent of the local dust plume over Adventdalen and the aerosol offshore the westcoast of Svalbard (Dörnbrack et al., 2009)

– combined data analyses of airborne AMALi lidar, ground based KARL lidar, ground based remote and in situ instrumentation at the research stations in vicinity of Ny-Ålesund on Svalbard (Stachlewska, 2006b),

– alternated AMALi and in-situ measurements of cloud structures and mixed-phase cloud optical and microphysical characteristics (Stachlewska et al., 2006c), (Gayet et al., 2007),

– investigation of a subvisible midlevel Arctic ice cloud with combined lidar, in situ and radiation instruments (Lampert et al., 2009a),

– investigation of boundary layer mixed-phase clouds in different air masses (Richter et al., 2008),

- identification of cloud phase from airborne spectral reflection measurements (Ehrlich et al., 2008),

- observations of boundary layer, mixed-phase and multi-layer Arctic clouds during ASTAR 2007 (Lampert et al., 2009b)

5   This paper gives a detailed description of the AMALi lidar, performance of the past and the present state of the system, as well as discusses the routine evaluation schemes applied to the airborne data.

2   Instrument description

The AMALi is a small, robust and easy to transport backscatter and depolarization lidar.
10 It is used for the remote high resolution detection of the vertical and horizontal extent of tropospheric aerosol load and clouds at two wavelengths and the depolarization at one wavelength simultaneously.

The lidar is mounted in two small, portable modules. The transmitting and receiving subsystems are mounted inside a small (70×50×25 cm) and light weight (45 kg)
15 module called the optical assembly (Fig. 1, left). The second module (Fig. 1, right) comprising the laser control and cooling unit, the data acquisition subsystem (laptop and transient recorders) and the safety breaker box is mounted in a standard size rack (55×50×60 cm).

The optical assembly module was especially designed and constructed by the Lidar
20 Group of AWI Potsdam with a constraint on the choice of the lidar components in a way to assure the lowest weight, space and energy consumption for the operation on board the Dornier Do 228 Polar 2 research aircraft. The optical assembly was manufactured by Steingross Feinmechanik, Berlin.

All vital lidar parts, i.e. the Nd:YAG laser head, the directing optics, the receiving
25 off-axis telescope mirror and the detector block with its opto-electronic elements are mounted onto the same optical bench inside the optical assembly. In Fig. 3 on the left,

the configuration deployed in 2003–2006, and on the right the present configuration are shown. The single-optical-bench design simplifies the adjustment of all optical elements and ensures reliable and trouble-free utilization during campaigns, without the need of re-adjustment. The optical bench itself hangs on anti-shock springs attached
5 to four posts. The springs eliminate vibrations of the optical bench during the operation on board of the aircraft. The weight and position of all elements (on the optical bench) are chosen in a way that the center of gravity results in the middle of the optical assembly. The four posts together with a base plate form a massive construction providing mechanical stability to the system. During measurements the optical assembly is cov-
10 ered with a sheet metal box capturing any scattered laser light and thereby ensuring the safety of pilots and operators, as well as protecting the detection system from stray light and background radiation.

The design of AMALi allows downward and upward measurements in vertical direction for the current configuration on board the Polar 2 and Polar 5 aircraft (Fig. 2). When
15 the lidar is operated at the ground level or integrated in a car or a ship, measurements are taken vertically upward. Horizontal measurements are possible for the optical system lying on a side. The lidar potentially can be used in a scanning mode, if it is set on a platform allowing movement of the whole system in a vertical/horizontal direction.

2.1 Transmitter subsystem

20 As a transmitter, a custom designed small rugged and easy to handle flashlamp pumped Nd:YAG pulsed laser (CRF-200, Big Sky Quantel, Montana, USA) is used (Table 1). It is provided with portable power supply and cooling unit mounted in a single, low weight (3 kg) and small unit, with space requirements of 12×45×48 cm. The laser, equipped with frequency doubler and tripler crystals, emits simultaneously two
25 wavelengths. The double wavelength backscatter lidar scheme was chosen for its conceptual simpleness ensuring an easy and trouble-free operation during field campaigns under tough Arctic conditions. The laser is cooled with an ethylene glycol and water 1:1 solution to ensure that the liquid will not freeze while the laser is operating under

Arctic weather and at high altitudes.

The maximum nominal operation height for the laser given by the manufacturer is 3 km. In the years 2003–2006 the two first harmonics were used, i.e. 1064 nm and linearly polarized 532 nm wavelengths with 11 ns short light pulses with energies of 60 mJ and 120 mJ, respectively, emitted with the pulse repetition rate of 15 Hz. The laser beam divergence δ is 2.6 mrad for 532 nm, and the diameter of the laser beam at the laser head g_0 is 6 mm.

After 2006 the second and third harmonics are used, i.e. linearly polarized 532 nm and linearly polarized 355 nm wavelengths with 11 ns short light pulses with energies of 94 mJ and 15 mJ, respectively, emitted with the pulse repetition rate of 15 Hz. The residual energy of the basic wavelength of 1064 nm (less than 45 mJ) is absorbed in the housing box by a white ceramic glass absorber material called Macor. Due to non perfect linear polarization, which came along with the implementation of the tripler crystal, a dual wavelength waveplate (CVI Laser, USA) and a Glan-Taylor polarizer (OFR, USA) are included in the optical assembly in the tube which is guiding the laser pulses through a hole in the telescope mirror. The waveplate is specially designed for 532 nm and 355 nm and shifts the polarization of the 532 nm wavelength by lambda/2 to match the polarization of the 355 nm wavelength, shifted by lambda. The Glan-Taylor prism acts as a polarization filter, passing only linear polarized light into the atmosphere. The perpendicular polarization is absorbed in the tube. The field of view in the UV is spherical as well. The exact divergence of the UV pulse was not measured but it was estimated by the manufacturer as 1.5 to 2.5 mrad, based on the measurement of the divergence for the 532 nm.

2.1.1 Detection range limitation

Despite its relatively small size, AMALi in a ground based configuration is powerful enough to cover the range up to the tropopause level. For airborne measurements its range is limited in two ways.

The detection range during the airborne measurements in nadir configuration is limited on the one hand by the maximum nominal operation height for the laser (up to 3 km), and the maximum allowed flight altitude without using oxygen masks by the pilots and scientific crew (up to 3 km for the installation in the Polar 2 and Polar 5 aircraft). On the other hand by the eye-safety constraints, i.e. above 2.5 km for the previous configuration, 2.1 km for the current configuration (Sect. 2.1.2).

In the case of the zenith-aiming airborne configuration, signals are limited on the one hand by the maximum nominal operation height for the laser (up to 3 km), and the allowed flight altitude (any altitude between 0–3 km). On the other hand by the maximum detection range which depends on the required signal to noise ratio (SNR), thus the integration time.

The Arctic tropopause level (typically at 9 km altitude in spring, and up to 11 km in summer) can easily be reached with an integration time of some minutes. The integration time depends on the altitude of the interesting structures. For zenith-aiming cloud observations in 4 km altitude, an integration time of 15 s is used. For reaching the tropopause with a sufficient SNR, longer averaging of some min is necessary.

2.1.2 Eye-safety constraints

To ensure the eye-safety of operators and pilots during the AMALi operation inside the aircraft the laser emitting subsystem is covered with the sheet-metal box mounted directly onto the optical assembly. The laser light is sent to the atmosphere through an opening of 15 cm diameter in the floor of the Polar 2 aircraft (nadir-aiming configuration) or through a similar opening in the roof (zenith-aiming configuration). In this case, the laser beam is covered by a light metal tube all the way from the optical unit to the hole in the roof. In both cases the laser light is sent out in an almost perpendicular direction to the long-axis of the aircraft.

To ensure the eye-safety outside the aircraft neither filters nor a beam expander are used. For the laser working at a full energy and simultaneously emitting two wavelengths, the large laser beam divergence ensures that the laser light is eye-safe at

AMALi

I. S. Stachlewska et al.

⏮ | ⏭

◀ | ▶

Back | Close

Full Screen / Esc

Printer-friendly Version

Interactive Discussion

distances greater than 2.5 km (2.1 km) off the lidar system for the past (current) configuration.

The eye-safety calculations were performed for both configurations separately. The values of Maximum Permissible Exposure (MPE) for direct viewing into the laser beam are specified in the document describing the regulations for the safe laser operations according to the German law (Sicherheitstechnische Festlegungen für Lasergeräte und Anlagen, 1998).

The MPE value depends on the pulse energy, pulse duration, wavelength, and beam divergence. Table 2 gives the MPE formulas for the calculations under the assumption that the laser can be considered a point-source of radiation (this can be assumed for the AMALi due to the only 6 mm small diameter of the laser beam at the laser head). Table 1 gives the specifications of the laser utilized in the AMALi system.

In the initial nadir-aiming configuration from 2003 till 2006 infrared (IR) and visible (VIS) pulses were emitted from the aircraft flying at the maximum permissible altitude of 3 km at the minimal crusing speed of 66 m s^{-1}. For this altitude and the laser beam divergence of 2.6 mrad the laser foot-print on the ground/sea expands to 7.8 m diameter and covers a surface of 47.78 m^2. For the minimum crusing speed of 66 ms^{-1} and the laser repetition rate of 15 Hz the centres of the two following laser-footprints are separated by 4.4 m from each other on the ground. Hence, a motionless observer can look into 2 consecutive laser pulses at most. For greater speed of the aircraft this number reduces.

Due to the similar pulse divergence and length of the 1064 nm and 532 nm pulses their exposure effect is additive. The actual exposure for both wavelengths must remain below the MPE value and satisfy all three following criteria (Table 2):

1. The exposure to one single pulse in the pulse-sequence cannot exceed the MPE value calculated for the direct exposure of the eye to the laser pulse. The $MPE^1_{532}=5\times10^{-3}\,Jm^{-2}$ and $MPE^1_{1064}=50\times10^{-3}\,Jm^{-2}$. The actual exposure for a 532 nm pulse with energy of 120 mJ for the footprint surface of $47.78\,m^2$ is $E^1_{532}=2.5\times10^{-3}\,Jm^{-2}$, and for a 1064 nm pulse with energy of 60 mJ is $E^1_{1064}=1.26\times10^{-3}\,Jm^{-2}$. The quotients of the actual exposure and the MPE values are 0.50 for 532 nm and 0.025 for 1064 nm.

2. The mean exposure to the duration of the pulse-sequence cannot exceed the MPE value for a pulse-sequence duration. In our case the exposure duration t is 0.13 s (2 incident pulses sent with 15 Hz repetition rate), so that the $MPE^2_{532}=3.97\,Jm^{-2}$ and $MPE^2_{1064}=19,48\,Jm^{-2}$. The actual exposure averaged for pulse-sequence is $E^2_{532}=2.51\times10^{-3}\,Jm^{-2}$ and $E^2{}_{1064}=1.26\times10^{-3}\,Jm^{-2}$. The quotients of the MPE and the actual exposure are 0.63×10^{-3} for 532 nm and 0.06×10^{-3} for 1064 nm.

3. The exposure to one single pulse in the pulse-sequence cannot exceed the MPE value calculated for the first criteria but multiplied by the correction factor $N^{-0.25}$, were N is number of the pulses in the pulse-sequence. For the 2 incident pulses the $MPE^3_{532}=4.2\times10^{-3}\,Jm^{-2}$ and $MPE^3_{1064}=42\times10^{-3}\,Jm^{-2}$. The actual exposure is $E^3_{532}=2.5\times10^{-3}\,Jm^{-2}$ and $E^3_{1064}=1.26\times10^{-3}\,Jm^{-2}$. The quotients of the MPE and the actual exposure are 0.595 for 532 nm and 0.03 for 1064 nm respectively.

For all three criteria the sum of the quotients is less than 1, so that the eye-safety criteria can be considered as passed. The quotient value obtained for the third criterion is the highest one, and hence it constrains the AMALi operation. For the operation of the AMALi under the typical measurement conditions the exposure is below the MPE values of $4.2\times10^{-3}\,Jm^{-2}$ for 532 nm and $42\times10^{-3}\,Jm^{-2}$ for 1064 nm. The third criterion was used to calculate the minimal permissible height of the eye-safe measurements performed in the nadir-aiming configuration. It is obtained by multiplying the maximum

permissible operation height by the square root of the final quotient of the third criterion (0.625), as the exposure intensity is proportional to I/r^2. Hence, the permissible height of the AMALi eye-safe operation in the nadir aiming configuration is between 2372 m and 3000 m.

For the present AMALi configuration the VIS and ultraviolet (UV) pulses are emitted into the atmosphere. For the 355 nm, the MPE is higher than for the 532 nm, as the eye is less sensitive in the UV spectrum. The MPE values are based on calculations with an aperture of 1 mm diameter in the UVA, and 7 mm in the VIS wavelength range. For the exposure with two wavelengths, one in the VIS, one in the UVA range, the values do not have to be treated additively. For a flight altitude of 3000 m, the diameter of the UV laser spot on the ground is 4.5 m, the area of the spot is 15.90 m^2. The pulse energy was assumed to be 25 mJ in the eye safety calculations, as specified in the laser data sheet, but this value constitutes an unrealistically high upper limit. As discussed above for the past AMALi configuration, a ground-based observer can be met by no more than 2 laser pulses. The MPE value for one single laser pulse and for the averaged pulses is 56 Jm^{-2}. The exposure of one UV laser pulse results in 1.57×10^{-3} Jm^{-2}, the averaged exposure is even lower. Thus exposure in the UV wavelength is more than 3 orders of magnitude below the MPE value. In the new AMALi configuration, the limitation of operating altitude in nadir configuration results only from eye safety considerations of the VIS wavelength. As in the past configuration, the third criterion is limiting for the eye safety. The same calculation as above leads to a minimum flight altitude of 2070 m.

Safe operation of the AMALi is achieved by switching on the laser only after the aircraft reaches the minimal height and when the safety shield is locked and fully covers the laser emitting subsystem.

2.2 Receiver subsystem

The optical layout of the receiver is composed of all signal collecting parts attached to the bottom of the optical bench. In the AMALi system, it is not necessary to use an aperture that is completely rotationally symmetric, and hence we could use the

off-axis optics to minimise the system size, weight and costs, and at the same time, to maximise its efficiency. The use of the off-axis configuration frees the system from astigmatism, while the use of the aspherical, parabolic mirror frees the system from spherical aberrations.

To collect the backscattered light, we use the off-axis parabolic mirror coated with protected silver coating (OAP 18-05-04Q, Space Optics Research Labs, USA). The mirror diameter is 10.2 cm and the clear aperture 9.9 cm. The focal length is 48.0 cm, while the off-axis distance is 12.7 cm. The mirror surface accuracy is high with figure (defines mirror roughness) of λ/10 wave peak to valley at 632.8 nm over 99% of the clear aperture and slope (defines mirror shape) of λ/8 waves per inch at 90%. The high reflective (near-UV, VIS and near-IR spectra) silver coating is a soft chemical surface with low durability, damage threshold and oxidation tarnishing. Hence, the silver layer is additionally over-coated with a hard, single, dielectric layer of half-wavelength optical thickness at 550 nm. This protective film arrests oxidation, helps maintain high reflectance, improves the minor abrasions and tarnish resistance, while only marginally affecting the optical properties.

The off-axis primary mirror is mounted onto the optical bench in a way that the laser light is sent through its central perforation of 3.1 cm diameter. The plane secondary mirror is mounted on a rod which is also attached to the optical bench. Similarly, the detector block with its opto-electronic elements, each placed inside one of the detection module-boxes (Fig. 3), is also attached to the optical bench. The light collected with the primary mirror is redirected by the first folding mirror onto a 1.5 mm pinhole on the detector block. Such a choice of pinhole size together with the parameters of the primary mirror results in 3.1 mrad field of view, necessary for the detection of the complete return signal of the strongly divergent laser beam. After passing the pinhole the light is redirected using the second plane folding mirror to an achromatic lens used to produce parallel rays while avoiding chromatic aberration.

In the AMALi configuration between 2003–2006 the signals of both wavelengths were separated into two different detection channels using a dichroic mirror inclined at 45°

which transmitted the 1064 nm and reflected the 532 nm signal. In the new configuration, a dichroic mirror was used which transmitted the 355 nm and reflected the 532 nm signal. For both configurations, the latter wavelength was additionally separated into its parallel and perpendicular component using a polarising cube beam splitter. In front of the photo-detectors interference filters (IF) were placed to reduce the background daylight radiation. For the IR channel we used a 1.0 nm wide IF centred around 1064 nm and for both VIS channels a 0.15 nm IF centred around 532 nm. For the UV channel, an IF of 1.0 nm bandwidth centred around 355 nm was employed. Due to the strongly limited range of the nadir-aiming airborne signals a high peak of the ground return occurs. However, the use of absorptive neutral density filters to reduce the intensity of the incoming light was not necessary. The less intense, perpendicular component of the 532 nm channel is additionally filtered for cross-talk using a thin film polarising filter at a 56° angle. In the new configuration with the more sensitive photon counting mode, neutral density filters were integrated in front of the photomultipliers for the 532 nm parallel and the 355 nm signal to avoid saturation of the detectors. The optical depths of 1.0 and 0.8, respectively, were chosen in a way that the output voltage of the photomultipliers was not at the limit for more than the first 50 m of the lidar signal return.

2.2.1 Overlap

Bearing in mind the laser pulse energy, the pulse repetition rate, the laser beam divergence δ, the beam diameter at the laser head g_0, and the primary mirror diameter T we chose the pinhole diameter s with the constraint to achieve the lowest possible geometric compression ξ (Sect. 3.1) with the lowest integration times for the weakest detection channel during the airborne nadir-aiming operation (i.e. perpendicular 532 nm).

To achieve the lowest possible geometrical compression we integrated an overlap-adjustment module just after the laser head. A double plain mirror, with high reflectance for the two lidar wavelengths in use is mounded onto a piezo stepper motor at an angle of approximately 45°. This mirror redirects the laser beam through the opening in the

optical bench on which the laser head is resting and sends it almost parallelly to the optical axis of the receiving telescope mirror. The distance between the telescope optical axis and the laser beam axis d_0 is set to 7.5 mm. Such construction allows fine adjustments of the overlap between the emitted laser beam and the telescope's mirror field of view φ. The complete overlap at a full field of view (Fig. 4), calculated analytically for the small θ, φ and δ angles approximation, follows $\xi = \frac{2\,d_0 + T + g_0}{2\,\theta + \varphi - \delta}$. For the AMALi the overlap ξ is completed at a distance of 235 m, when the laser beam is not inclined ($\theta = 0$). Inclination of the laser beam to the maximum applicable inclination angle ($\theta = \frac{\varphi - \delta}{2}$) of 0.27 mrad results in ξ_{min} of 155 m.

2.3 Data acquisition subsystem

The lidar system provides high spatial/horizontal resolution information on the state of the atmosphere between the flight altitude and the ground/sea level or the tropopause during the measurement. The rapid data acquisition system enables recording of lidar profiles with single-shot resolution.

A single laptop computer (TOSHIBA, 2 GHz, CPU 30 GB, HD 256 MB RAM, USB-RS 232, Windows XP-Pro, OPS English) fully controls the laser, transient recorders, detectors, and data acquisition, including storage, processing, quick-look evaluation and display programs utilizing LabVIEW software. As data acquisition system a transient recorder (TR20-80, LICEL GmbH, Berlin) combining an A/D converter (12 bit at 20 MHz) for analog detection with a 250 MHz fast photon counting system are used. An ethernet control module using a TPC/IP protocol allows remote control and data transfer for both photon counting and analog recorders. For the detection of the 1064 nm channel a Peltier cooled Si Avalanche Photo-Diode (APD) was used, and Hamamatsu R7400 photomultipliers (PMT) for the detection of the 355 nm channel and the two 532 nm channels for the parallel and perpendicular component. Transient recorders register the pulses with a maximum sampling rate of 20 MHz corresponding to a height resolution of 7.5 m for one range bin.

AMALi

I. S. Stachlewska et al.

In the zenith-aiming ground-based configuration the standard ground-based LICEL data acquisition software is employed. Here each new lidar return signal from each channel is stored separately at a time average of minimum 1 s and hence, a single-shot acquisition is not possible. With this standard software the profiles up to the tropopause level can be easily obtained.

In the nadir and zenith aiming airborne configuration a custom designed airborne LICEL software is employed. Typically each new lidar return signal from each of the three channels is appended and stored with a temporal integration of 1 s per profile in a block file of 2 min. However, a resolution as fine as a single-shot acquisition is also possible.

For nadir measurements from 2003–2006, the length of each collected signal was limited to 1000 range bins (7.5 km) to decrease the time needed for data transfer between transient recorder and the laptop (smaller size of data files). At the same time, this provided sufficient number of bins for the required range determined by the altitude of the flying aircraft for nadir-aiming configuration, i.e. maximum of 3 km above sea level. For this short distance (significantly shorter than the zenith-aiming ground based range), a strong received signal with sufficient signal-to-noise ratio is guaranteed, so that the photomultipliers can be operated in an analog mode only (Goodman, 1985).

It is worth to note that measurements in a nadir-aiming airborne configuration generally provide a better signal-to-noise ratio at a far distance from the aircraft, as the measured aerosol concentration and the air density increase towards the ground. On the other hand, for the airborne applications only short integration times are allowed in order to achieve a sufficient horizontal resolution. An acceptable signal-to-noise ratio for the available measurement range of 3 km on board the Polar 2 is achieved for an integration time of 1 s. This corresponds to a horizontal resolution between 46 m and 77 m at a minimum of 166 km h^{-1} and maximum of 278 km h^{-1} aircraft cruising speed over ground, respectively.

In the new configuration designed for also zenith-aiming airborne applications, the signal length was set to 1700 bins, which is close to the limit for data transfer. The detectors are read out simultaneously in analog and photon counting mode to increase the measurement range and to compensate the effect of the neutral density filters which

5 reduce the signal intensity. For the evaluation of cloud systems, an integration time of 15 s was generally chosen. This resulted in an acceptable SNR above 15 at a distance of 4.5 km from the aircraft, and a horizontal resolution of about 900 m for the typical cruising speed of the Polar 2 of 66 ms^{-1}.

2.4 Quick-look data processing and display

10 The acquired airborne data can be viewed online directly during the flight using the especially designed, so called quick-look data evaluation screen in the data acquisition programs. Exemplary quick-look real-time evaluation displays obtained during one of the flights in a mixed-phase cloud system are shown in Fig. 5. Each second one display screen provides all three currently measured raw signal profiles. Similarly, three

15 other screens are frequently updated displaying time series of background and range corrected signal profiles at both 1064 nm and parallel 532 nm channels, as well as with depolarization ratio profiles (defined as a ratio of the 532 nm perpendicular signal to the 532 nm parallel signal), all averaged over 15 s. For the new configuration, the display of raw lidar backscatter profiles of all three detection channels in both analog

20 and photon counting mode is updated every second. The representation of each of the six profiles can be switched on and off separately in order to have an overview of the performance of all signals or to concentrate on the channel of interest. The three displays for background and range corrected time series can represent optionally any of the six signals or ratios of the signals. According to the structures of interest,

25 this may be the analog or photon counting signals, the depolarization ratio (532 nm perpendicular to 532 nm parallel signal) or the colour ratio (532 nm to 355 nm signal). Examples of quick-look displays for two cases are represented in Fig. 6. The upper pictures are nadir observations of precipitating mixed-phase clouds, the lower pictures

show zenith observations of a subvisible ice cloud.

The real time, quick-look data evaluation software allows immediate qualitative interpretation of the aerosol content and clouds during the flight. This "first-guess" information is sufficient for an on board lidar operator to guide another research aircraft for specific measurements. For example during the ASTAR 2004 campaign this quick-look evaluation feature allowed to guide alternated Polar 2 in situ measurements. In this case after the remote identification of particularly interesting regions in mixed-phase clouds (indication of height and relative concentration of water droplets and/or ice crystals areas) by lidar measurement, the aircraft descended into the specified sections of these clouds to perform the in situ measurements of their microphyscial and optical parameters (Gayet et al., 2007). During the ASTAR 2007 campaign, the AMALi detected a thin ice cloud at an altitude of around 3 km in zenith aiming configuration, which was invisible to the eye. The aircraft returned to the location at the altitude indicated by lidar observations, and the in situ measurements were able to probe single ice crystals (Lampert et al., 2009a).

3 Lidar equation and data evaluation algorithms

The AMALi lidar provides users with a high quality information on the existence, altitude distribution, backscatter and depolarization of the vertical and horizontal extent of tropospheric aerosols and clouds of a low optical thickness. It delivers profiles of the range and background corrected signals, the aerosol backscatter coefficient, the aerosol particle non-sphericity (depolarization information). Finally, by the remedy of additional information or instrumentation, even the extinction coefficients can be retrieved.

In the following two sections the evaluation schemes applied on a routine basis to the AMALi data are discussed.

3.1 Lidar equation

The elastic lidar equation describes the received signal as a function of the atmospheric and system parameters, whereby assumptions of quasi-monochromatic coherent emitted laser light and instantaneous elastic or inelastic scattering are taken into account, while processes of multiple scattering of light are being neglected (Shimoda, 1986). The lidar equation is usually used in a form of the range corrected signal $S(h, \lambda)$, obtained by multiplication of the detected signal with the squared range vector (Eq. 1)

$$S(h, \lambda) = P(h, \lambda)h^2 = C\xi(h)\beta(h, \lambda)T^2(h, \lambda) \tag{1}$$

where λ denotes the emitted wavelength and h the distance between the lidar and the target particle or molecule. The detected signal $P(h, \lambda)$ is proportional to the mean number of photons c with the photodetector, i.e. the intensity of the detected wavelength dependent backscattered signal at a time $t=2h/c$. The geometrical efficiency of the detection system $\xi(h)$ is dependent on the geometrical compression, called also overlap function. The geometrical compression term vanishes if the solution of the lidar equation is found at the range h_{gc} beyond which the recorded signals are free of the geometrical compression, i.e. $\xi(h \geq h_{gc})=1$, due to the fact that from this range the emitted laser beam is entirely seen by the full field of view of the telescope (Sect. 2.2.1).

The term $T(h, \lambda)$ describes, accordingly to the Lambert-Bouguer-Beer's law, the transmission of the laser energy through the atmosphere, which yields an exponential attenuation of the laser radiation due to the optical mass and optical depth $\tau^{tot}(\lambda)$ of all molecules $\tau^{mol}(\lambda)$ and particles $\tau^{part}(\lambda)$ present in the atmosphere on the way of the laser beam. Hence, $T(h, \lambda)$ depends on the extinction $\alpha(h, \lambda)$ of the signal due to the scattering and absorption on the way from the source of lidar radiation to the range h and back (Eq. 2)

$$T(h, \lambda) = \exp\left(-\int_{h_0}^{h} \alpha(\tilde{h}, \lambda)d\tilde{h}\right) \tag{2}$$

$\beta(h, \lambda)$ and $\alpha(h, \lambda)$ denote the total backscatter and the total extinction coefficients depending on the total number of molecules and particles scattering and/or absorbing the laser light at the height h above ground (Eqs. 3 and 4).

$$\beta(h, \lambda) = \beta^{\text{mol}}(h, \lambda) + \beta^{\text{part}}(h, \lambda) \tag{3}$$

$$\alpha(h, \lambda) = \alpha_{\text{scat}}^{\text{mol}}(h, \lambda) + \alpha_{\text{scat}}^{\text{part}}(h, \lambda) + \alpha_{\text{abs}}^{\text{mol}}(h, \lambda) + \alpha_{\text{abs}}^{\text{part}}(h, \lambda) \tag{4}$$

By the choice of the emitted laser wavelength in a way that most of the atmospheric constituents do not absorb it and, hence, the favorable SNR is obtained even at high altitudes, the absorption term in the definition of the molecular extinction coefficient can be neglected ($\alpha_{\text{abs}}^{\text{mol}}(h, \lambda) \approx 0$). The backscatter and extinction coefficients split to only two scattering dependent terms; the molecular terms $\beta^{\text{mol}}(h, \lambda)$ and $\alpha^{\text{mol}}(h, \lambda)$ due to the existence of the gaseous constituents of the atmosphere (Rayleigh scattering) and the particle terms $\beta^{\text{part}}(h, \lambda)$ and $\alpha^{\text{part}}(h, \lambda)$ due to the existence of aerosols in the atmosphere (Lorenz-Mie scattering).

3.1.1 Lidar constant

The terms describing the range independent parameters of the lidar system appear in the definition of the lidar instrumental constant C which, at least theoretically, can be calculated or found experimentally for any individual lidar (Eq. 5).

$$C = P(h_0, \lambda) \xi(\lambda) \Delta h A \tag{5}$$

The mean number of photons in the emitted laser pulse $P(h_0, \lambda)$ corresponds to the intensity of the wavelength dependent laser pulse emitted at a time t_0. The spectral efficiency of the detection system $\xi(\lambda)$ depends on spectral efficiencies of the photo-detectors and the spectral transmittance of the optical elements. A denotes the effective telescope surface, and then A/h^2 is the solid angle of signal collection. Finally, Δh describes the spatial resolution of the system, which is determined by the laser pulse duration τ by definition. In reality it is limited by the slowest component of the system (photomultiplier efficiency or transient recorder speed) and hence always $\Delta h \gg c\tau/2$.

3.2 Depolarization ratio

Measurements of the depolarization ratio provide information to discriminate between spherical and non-spherical particles in the atmosphere. Hence, such measurements can be helpful in distinguishing between liquid and solid phase particles.

If a lidar system detects simultaneously the backscattered light polarized in parallel and perpendicular direction with respect to the emitted laser beam, the total volume depolarization ratio DR, i.e. the depolarization induced by atmospheric particles and molecules can be obtained (Eq. 6).

$$DR(h,\lambda)=DR^{\mathrm{mol}}(h,\lambda)+DR^{\mathrm{part}}(h,\lambda)=\frac{P_{\mathrm{perp}}(h,\lambda)}{P_{\mathrm{par}}(h,\lambda)} \tag{6}$$

As the detection of both the $P_{\mathrm{perp}}(h)$ and $P_{\mathrm{par}}(h)$ signals is done using two different opto-electronic detection channels characterized with a different gain, both measured signals must be well calibrated to provide high quality measurements (Sect. 5.1).

4 Qualitative and quantitative data analyses

The range corrected signal (Eq. 1) provides the lidar user with a qualitative information (so called first type end-product) on the existence and altitude distribution of aerosols and clouds of a low optical thickness.

The quantitative information (so called second type end-product) can be obtained via inversion of the lidar signals and calculation of the profiles of the particle backscatter $\beta^{\mathrm{part}}(h,\lambda)$ and the particle extinction $\alpha^{\mathrm{part}}(h,\lambda)$. The main difficulty of such an inversion is caused by the existence of two unknowns (α and β) in one lidar equation (Eq. 1), so that no unique solution can be found. The assumptions and estimations made to find the solution of the lidar equation for the ground based and airborne measurement configuration are discussed in Sect. 4.1 and Sect. 4.2, respectively.

AMALi

I. S. Stachlewska et al.

Title Page

Abstract | Introduction

Conclusions | References

Tables | Figures

◀◀ | ▶▶

◀ | ▶

Back | Close

Full Screen / Esc

Printer-friendly Version

Interactive Discussion

4.1 Ground-based data evaluation

Until 2006, as a first type end-product of the zenith-aiming and the horizontal-aiming ground based lidar configuration, profiles of background and range corrected signal at 1064 nm and parallel 532 nm and profiles of depolarization ratio at 532 nm were deliv-
5 ered. The background correction (Sect. 5.1) for these data was done with a pretrigger and profiles were usually averaged with 1 s temporal and 7.5 m range resolution. For this averaging the zenith measurements easily reached the tropopause level and the horizontal measurements provided data up to a distance of 4 km. It is worth to notice that in the zenith configuration the cirrus cloud detection was achieved with only a few
10 pulses.

In the new configuration, the system delivers profiles of background and range corrected signal at 532 nm and 355 nm and profiles of depolarization ratio at 532 nm. The standard evaluation is done for a temporal average of 15 s and a horizontal resolution of 7.5 m with the pretrigger background correction (Sect. 5.1). For the measurements
15 of cirrus clouds at the far range from the lidar system, the neutral density filters can easily be removed.

Second type end-products, i.e. the backscatter and extinction coefficients, are calculated depending on the lidar configuration mode, as discussed in the two following subsections.

20 ### 4.1.1 Horizontally-aiming ground based inversion

For the horizontally-aiming ground based AMALi configuration the slope method (Klett, 1981) is used when the assumption of an aerosol rich homogeneous atmosphere can be made. In the case of the atmosphere rich in aerosol (e.g. in the planetary boundary layer), the contribution of aerosol particles to the measured backscatter and extinction
25 coefficients strongly exceeds the contribution of molecules. By defining the natural logarithm of the range corrected lidar signal as $S(h)=ln(S(h, \lambda))$ and neglecting the molecular terms $\beta^{mol}(h, \lambda)$ and $\alpha^{mol}(h, \lambda)$ the lidar equation can be rewritten for a single

wavelength (Eq. 7).

$$\frac{d}{dh}S(h) = \frac{1}{\beta^{\text{part}}(h)} \frac{d\beta^{\text{part}}(h)}{dh} - 2\alpha^{\text{part}}(h) \tag{7}$$

A unique solution to this equation does not exist since Eq. 7 still suffers from two unknowns, $\beta^{\text{part}}(h, \lambda)$ and $\alpha^{\text{part}}(h, \lambda)$. The slope method approach, however, provides a solution based on the assumption that the emitted laser light propagates in the homogeneous atmosphere. In this case changes of the backscatter coefficient in the interval dh are negligible ($\frac{d}{dh}\beta^{\text{part}}(h){=}0$) and the aerosol extinction coefficient can be directly calculated (Eq. 8).

$$\alpha^{\text{part}}(h) = -\frac{1}{2} \frac{d}{dh}S(h) \tag{8}$$

A typical extinction profile obtained with the slope method reaches 4 km for applied 1 min temporal and 7.5 m range resolution.

4.1.2 Zenith-aiming ground based inversion

For the zenith-aiming ground based configuration the Klett-Fernald-Sasano's backward approach is used (Klett, 1981, 1985; Fernald, 1984; Sasano et al., 1985).

In this case the assumption of the homogeneity of the atmosphere cannot be made, as the backscatter coefficient strongly changes throughout the troposphere. Additionally, for the heterogeneous atmosphere there are ranges where $\alpha^{\text{part}}(h)$ and $\alpha^{\text{mol}}(h)$ and $\beta^{\text{part}}(h)$ and $\beta^{\text{mol}}(h)$ are of the same order of magnitude, and hence the molecular contributions cannot be assumed negligible. However, they can be obtained (Sect. 5.1).

In the lidar equation (Eq. 1) two unknowns remain, the $\alpha^{\text{part}}(h)$ and the $\beta^{\text{part}}(h)$. To invert the equation an altitude dependent lidar ratio (Eq. 9) is assumed and the equation is solved with respect to the particle backscatter coefficient. Note that the

height independent lidar constant (Eq. 5) proves redundant in these calculations.

$$B(h, \lambda) = \frac{\alpha^{\text{part}}(h, \lambda)}{\beta^{\text{part}}(h, \lambda)} \qquad (9)$$

The backward inversion is performed starting with a point chosen far from the lidar, i.e. at the aerosol free range of the troposphere by calibration to the known molecular backscatter coefficient value or to the value of the particle backscatter coefficient known for the cirrus clouds (Ansmann et al., 1992), if such appear.

Finally the unitless backscatter ratio profiles are calculated (Eq. 10).

$$BSR(h, \lambda) = \frac{\beta^{\text{mol}}(h, \lambda) + \beta^{\text{part}}(h, \lambda)}{\beta^{\text{mol}}(h, \lambda)} \qquad (10)$$

The profiles typically obtained with the Klett-Fernald-Sasano's backward approach are evaluated for the periods of the measurement performed in cloudless conditions. With 1 min temporal and 7.5 m range resolution these reach the tropopause level.

4.2 Airborne data evaluation

As a first type end-product of the airborne lidar configuration, profiles of background and range corrected signal and depolarization ratio at respective wavelengths are performed. The profiles are usually averaged over 1 s with range resolution of 7.5 m and horizontal resolution of 67 m for typical aircraft's cruising speed over ground of 66 m s^{-1}. Typical length of airborne profile vary between 2.25–2.75 km (nadir-aiming) and 350 m–15 km (zenith aiming), depending on the actual flight altitude and taking into account the 155–235 m losses due to the geometrical compression near the lidar (Sect. 2.2.1). For the airborne measurements the background correction value for each profile is obtained from the pretrigger part of the signal and extracted from each profile separately (Sect. 5.1).

Second type end-products, i.e. the backscatter and extinction coefficients, are calculated differently depending on lidar configuration mode.

4.2.1 Zenith-aiming airborne inversion

For the zenith-aiming airborne data evaluation the Klett-Fernald-Sasano's backward approach with an assumption of the lidar ratio and a calibration at the tropopause level, in the free troposphere or at the cirrus cloud level is used (i.e. similarly as for the zenith-aiming ground based configuration discussed in Sect. 4.1.2). Typical averaging applied for these profiles depends on the aim of the measurements and the distance of the structures of interest. For example for the comparison of lidar profiles with space borne CALIOP, a temporal average of 15 s results in a similar horizontal resolution as the average of three single CALIOP profiles of about 1 km. Cirrus clouds up to 6 km altitude can be evaluated using this resolution. A 1 min temporal and 7.5 m range resolution results in calculation range up to the Arctic tropopause level.

4.2.2 Nadir-aiming iterative airborne inversion

The standard Klett-Fernald-Sasano's backward approach described in Sect. 4.1.2 cannot be used straight forward for the data evaluation of any nadir-aiming airborne elastic lidar measuring alone in the lower troposphere. The main problem of using the standard scheme arises from the difficulty of providing the calibration value for each of the profiles. The lowermost part of the troposphere is usually rich in turbulent aerosol particles generated by surface winds. In these areas the backscatter coefficient is highly variable during the flight and hence it is very difficult to estimate, since the phase function dependence with height has to be accounted for. It is similarly difficult to provide any reference backscatter values in the low troposphere due to the lack of aerosol free layers. Also the limited signal range between the flight altitude and ground/sea level adds to the signal calibration problem.

Here we present an improved iterative approach for the calculation of the backscatter coefficient profiles from the airborne elastic backscatter lidar data, independent of the existence of aerosol free layers or in situ calibration measurements. Using this approach the backscatter coefficient profiles are calculated from these profiles using an

assumption of the lidar ratio $B(h)$. The application of this new approach allows to provide the profiles of calibrated backscatter ratios $BSR(h)$ at any time during the whole flight. A typical backscatter coefficient profile obtained with this method is averaged over 15 s with 7.5 m range resolution and 1 km horizontal resolution for 66 ms^{-1} t aircraft's cruising speed over ground. Examples of the application of this method can be found in (Stachlewska and Dörnbrack, 2006a; Stachlewska, 2006b; Stachlewska et al., 2006c; Gayet et al., 2007; Dörnbrack et al., 2009).

The iterative approach is described here in the following steps.

For a known lidar constant C and a short (few hundred meters) range h_{gc} at which the geometrical compression is completed $\xi(h \geq h_{gc})=1$ (in the case of the AMALi h_{gc} is approximately 250 m), the assumption of a negligible attenuation of the emitted laser light along the flight altitude h_f and geometrical compression h_{gc} can be done (Eq. 11).

$$T_{[h_f,h_{egc}](h,\lambda)} \approx 1-(h_f-h_{gc}) \cdot \alpha(h_f) < 1 \qquad (11)$$

By neglecting the transmittance term the backscatter at the altitude h_{gc} can be estimated for each time step during the flight (Eq. 12).

$$\beta(h_{gc}) > \frac{S(h_{gc})}{C} \qquad (12)$$

The knowledge of $\beta(h_{gc})$ for all times during the flight allows now for an application of the standard Klett-Fernald-Sasano's backward procedure with the following constraints. The backscatter coefficient calibration value $\beta_{KFS}(h_{ref})$ is chosen in a far distance from the lidar (i.e. near the ground/sea level for the nadir-aiming AMALi). It is set in a way that the value of the backscatter coefficient $\beta_{KFS}(h_{gc})$ calculated using the Klett-Fernald-Sasano's backward inversion at the height corresponding to the completed geometrical compression, matches the estimated value of $\beta(h_{gc})$. If these do not match the $\beta_{KFS}(h_{ref})$ is chosen again, accordingly to the iterative Newton-Raphson method, until the two values are the same.

The clearer the atmosphere and the better α^{mol} is known, the better the transmittance of the layer $[h_f, h_{gc}]$ can be estimated and the error of $\beta(h_{gc})$ decreases. Hence, such

an iterative approach provides β profiles which are calibrated during the whole flight and α profiles calculated as precise as the choice of the lidar ratio $B(h)$ (Sect. 5.3).

4.3 Combined nadir-aiming and zenith-aiming inversion

Another evaluation method can be applied for each time period when the nadir-aiming lidar overflies a zenith-aiming lidar system. In our case the combined evaluation of the data obtained from the AMALi lidar overflying the Koldewey Aerosol Raman Lidar (KARL; Ritter et al., 2004) allows for the direct calculation of the extinction and backscatter coefficient profiles using the two-stream approach (Stachlewska et al., 2005; Ritter et al., 2006; Stachlewska and Ritter, 2009). Typically such profiles are calculated with 8–10 min temporal resolution and 60 m horizontal resolution. The range of these profiles is strongly determined by the altitudes where the method is applicable, i.e. the atmosphere above the geometrical compression of the ground-based zenith aiming lidar and below the geometrical compression of the nadir aiming airborne lidar. The essential problem for the proper application of the two-stream method is the fact, that the both lidars must sample into the same atmosphere. The pre-selection of the appropriate signals can be done using the iterative correlation method (Ritter et al., 2006; Stachlewska and Ritter, 2009).

Similarly, the two-stream algorithm can be applied for each of the time periods when the zenith-aiming AMALi flies over a path of the nadir-aiming CALIOP lidar.

5 Measurement quality assessment and examples of data analyses

5.1 Lidar signal calibration and instrumental constant estimation

1) Background light correction

The lidar signals measured during daytime have to undergo a correction for the background stray-light photons, which are collected by the receiving subsystem together with the backscattered laser pulses. This correction is especially important in the polar regions where, due to the high albedo of ice and snow covering most of the sea and land, the background light intensity is unusually high.

For the zenith-aiming powerful lidars, which can record signals with sufficient signal-to-noise ratio even in the stratosphere, such a correction can be done using the highest range of their signals, where the assumption of collecting only background light and electronic noise is made.

The limited range of the recorded nadir-aiming airborne signals results in a difficulty to obtain the background light intensity, which has to be subtracted for any further data evaluation. To overcome this problem in the AMALi system, the data acquisition is started by an adjustable pretrigger prior to the laser Q-switch. It was designed by the LICEL GmbH especially for the AMALi airborne applications in the Arctic. The timing of the pretrigger was chosen as a value of $25\,\mu s$ corresponding to 500 range bins (3.75 km) of the signal for the applications to the nadir-aiming airborne measurements performed until 2006.

In the new configuration, a standard pretrigger delay of $20\,\mu s$ and $5\,\mu s$ was used for nadir- and zenith-aiming measurements, respectively. For the zenith evaluation, the background values can also be obtained from the signal values at far range, if no thick clouds, which cause multiple scattering, are present. However, the height of the background values at the far end depends on the integration time, and hence most of the time the pretrigger is used.

2) Rayleigh calibration

The calibration of the obtained lidar signals is done by normalizing them to the molecular elastic backscatter profile at an altitude range where the signal is only caused by the molecular contribution (so-called Rayleigh atmosphere). To obtain the particle backscatter and extinction coefficients, the profiles of the Rayleigh atmosphere are subtracted from the lidar profiles. They are calculated using the radiosonde data launched in the area nearby performed observations at a time interval of ±2 h from the AMALi measurements. If such radiosonding observations are not avaliable the molecular profiles are calculated from the the standard US atmosphere profiles. In the cases when the cirrus clouds appear in the troposphere the calculations are performed only up to the cirrus bottom height and calibrated in the cirrus region (Ansmann et al., 1992).

3) Depolarization ratio calibration

The total depolarization ratio is proportional to the ratio of the signals measured with the perpendicular and the parallel channel. Both signals have to be well calibrated to provide high quality measurements. This is done by instantaneous calibration using the normalization of the real signal to the molecular elastic backscatter one in an altitude range where the signal is only caused by the molecular contribution with a known and constant depolarization of 0.00376 (Behrendt and Nakamura, 2002). Usually the height interval in the free troposphere which appears to be clearest is used for the normalization, as the Arctic atmosphere generally is very clean. Also the cross-talk between the two channels needs to be accounted for. In our case both channels were checked for the cross talk in an experimental way, and it was found that cross talk is not an issue.

4) Lidar ratio assumption

The lidar equation itself (Eq. 1) well illustrates the difficulty of measuring optical properties with a classic elastic lidar. The instrument provides one single measure-
5 ment of backscattered power at each range which is dependent on the scattering cross section at that range and the two-way attenuation on the path to the scattering volume. Hence, the signal contains insufficient information to separately determine the scattering cross section and the optical depth. By making assumptions regarding relationships between the extinction cross section and the backscatter cross section,
10 i.e. the assumption of the lidar ratio (Sect. 4.1.2), a solution may be obtained. The direct measurements of the lidar ratio and its calculations from Mie theory show that the relationship between extinction and backscatter is highly variable, as it strongly depends on the highly variable size distribution of the scattering particles in the atmosphere. Hence, a wrong estimation of the lidar ratio is a dominant factor, that
15 causes ambiguity in the solution of the classic elastic lidar equation (Kovalev and Eichinger, 2004).

An accurate inversion can be made only if the lidar ratio is adequately estimated. Commonly used range-independent lidar ratio may be assumed only for an inversion of measurements taken in a horizontal direction, in a highly averaged sense over a
20 uniform flat ground surface, when there are no local sources of the atmospheric het-erogeneity present. For sloped or vertically directed measurements (strongly heteroge-nous atmosphere) the inversion can be made when the spatial behavior along the line of sight is known. In this case the estimation of the range-dependent lidar ratio is challenging unless an independent information on the extinction is obtained by the in-
25 elastic techniques, e.g. with the Raman scattering method (Ansmann et al., 1990) or High-Spectral-Resolution method (Shipley et al., 1983). In such cases the accuracy of the independently obtained information strongly depends on the quality of the inelastic measurement.

The assumption of the lidar ratio for the purpose of using the iterative airborne approach is discussed with the example of real data in Sect. 5.3.

5.2 AMALi intercomparison with KARL

For two measurements taken with two different lidars, at the same wavelength, time
and aim, and with application of the same profile averaging in time and space, their
signal statistics can still differ significantly due to differences in the emitted laser power
and field of view of their receiving telescopes (Matthias et al., 2002). The system
intercomparison is crucial to assess their ability to obtain the same results when the
same evaluation scheme is applied.

Intercomparison measurements of the AMALi and the KARL lidars were performed
with both systems operating simultaneously at 532 nm in a zenith-aiming ground based
configuration under clear-sky weather conditions typically chosen for lidar measurements. Observations were performed between 21:30–22:10 UT on 15 June 2004 from
the AWI atmospheric observatory at the AWIPEV research base in Ny-Ålesund. The
lidars were placed approximately 30 m apart to ensure that each laser beam and telescope field of view did not overlap. In such a configuration KARL's data were recorded
up to the tropopause and the AMALi's data up to 7.5 km.

The lidar signals were initially compared by simple division of background and range
corrected signals averaged to the same spatial (60 m) and temporal (5 min) intervals.
Afterwards, the backscatter ratio profiles were retrieved for both lidars using the same
evaluation scheme, i.e. the Klett-Fernald-Sasano approach described in Sect. 4.1.2.
However, the calculation was done under the assumption of a height independent lidar
ratio of 30 sr. The KARL's profiles were calibrated by setting a boundary condition in the
tropopause with backscatter ratio of 1.05. The AMALi's profiles were calibrated with a
backscatter ratio of 1.06 at the range free from the aerosol and cloud particles evident
in the recorded signals between 4.8–5.0 km.

AMALi

I. S. Stachlewska et al.

The temporal evolution of the backscatter ratio profiles for both lidars obtained for the whole observation period on that day is given in Fig. 7. On the same figure the profiles integrated over 20 min intervals (red and green) at 21:30 UT and 21:50 UT as well as the profiles integrated over the entire measurement period (blue and black) are presented. The agreement of KARL and AMALi retrievals is very good with deviations less than 3%. Stronger deviations, up to 30% at the range below 750 m occur due to the wrong adjustment of the KARL's near-range small telescope on that particular day, i.e. the KARL's backscatter ratio profiles are strongly underestimated in this range. The deviation in the backscatter ratio values at a layer between 1.4 km and 2.4 km altitude are caused by passing thin, subvisible clouds, well captured by both lidars. Already for 20 min integration time both lidar retrievals converge, i.e. deviations in this height interval are mainly due to the high temporal and spatial variability of these clouds. The condensation in this layer must be dominated by small scale processes with a life time of 20 min since the averaging of the lidar signals is just sufficient to smear them out.

Good agreement of the profiles above the mentioned KARL's lower range give evidence that both lidars obtain the same results. Noise in the signals and/or the detection efficiencies of both instruments are of no concern, giving confidence for the application of the two-stream evaluation of the data obtained with lidars operated in airborne nadir and groundbased zenith configuration.

5.3 Sensitivity study of the iterative airborne approach

For the calculation of calibrated lidar profiles of the backscatter coefficient during the whole flight, the approach described in Sect. 4.2.2 can be applied in cases when the calibration value cannot be estimated (lack of an aerosol-free layer) or cannot be provided a priori (from an additional on board in situ calibration instrumentation, and/or on board horizontal or vertical scanning of the emitted lidar light is not available). Unlike for the zenith-looking tropospheric lidars, generally, for the short-range nadir-aiming airborne lidar the largest term of the error propagation of the backscatter coefficient profiles is due to the wrong assumption/estimation of the backscatter calibration value

(partial derivative of backscatter over range). The wrong assumption of the lidar ratio contributes much less to the backscatter ratio uncertainty (small partial derivative of backscatter over lidar ratio).

In the case of the approach proposed in Sect. 4.2.2 the assumption of the transmittance term $T=1$ in the airborne lidar equation permits the accurate estimation of $\beta(h_{gc})$ in range intervals close to the lidar, i.e. at an altitude near the aircraft but beyond geometrical compression of the lidar. In case of the AMALi lidar, for the height chosen just below a geometrical compression of 235 m the expected error for neglecting the transmittance term varies from 0.7% for the particle extinction of $0.15\times10^{-4}\mathrm{m}^{-1}$ typical for clear Arctic atmosphere ($T\approx0.993$), up to 2.8% for the particle extinction of $0.6\times10^{-4}\mathrm{m}^{-1}$ for aerosol contaminated atmosphere ($T\approx0.972$). Hence, the clearer the atmosphere and the better the knowledge of the molecular contribution to the extinction α^{mol} (for example from nearby meteorological sounding) the better the transmittance estimate, i.e. the lower uncertainty of the $\beta(h_{gc})$ calculation. Furthermore, the accuracy of the α and β calculated with the iterative approach at any time during the flight depends mainly on the assumption of the lidar ratio since the error of the estimation of $\beta(h_{gc})$ near the aircraft (and dependent on it, iteratively found $\beta(h_{ng})$ near ground) hardly affects the error of the backscatter retrieval itself.

An example of the application of this iterative airborne inversion for the calibrated -along-flight- backscatter ratio profiles is depicted in Fig. 8. The data were obtained during a flight on 19 May 2004 during the ASTAR 2004 campaign. The backscatter ratio profiles (Fig. 8) were calculated with 15 s temporal resolution corresponding to 1 km spatial resolution. In case of thick clouds the backscatter ratio could not be retrieved due to multiple scattering. For these calculations the AMALi lidar instrumental constant C_A was obtained from the simultaneous measurements of AMALi and KARL taken during the AWIPEV Station overflights and $C_A=1.43(\pm0.1)\times10^{13}\,\mathrm{m\,V\,m^3\,sr}$. The lidar ratio profiles obtained from the KARL data at the Ny-Ålesund location showed mainly background values of the lidar ratio of 20 sr with a layer of extremely high values of the lidar ratio of 80 sr due to the existence of the aerosol layer of rather local origin. The

AMALi

I. S. Stachlewska et al.

Full Screen / Esc

Printer-friendly Version

Interactive Discussion

air mass transport calculated with the Hybrid Single-Particle Lagrangian Integrated Trajectory (HYSPLIT) model for that flight showed a non-uniform character, whereby a contamination with anthropogenic aerosol could not be totally excluded. Hence, the choice of the appropriate lidar ratio for calculations along the flight was not straight

5 forward. Therefore, the sensitivity study with respect to the estimation of the error due to the assumption of a different type of lidar ratio was performed. For the following constraints on the lidar ratio (Table 3) the error of the backscatter coefficient calculation was obtained, respectively.

Additionally, calculations were performed for the height dependent lidar ratio set to
10 35 sr between 0–1600 m and to 20 sr at 1600–2500 m, for which (within the given uncertainties in Table 3) the same values of the particle backscatter coefficients were obtained as for the results calculated with corresponding results of constant lidar ratios.

Performed sensitivity studies show no significant hindering of the iterative cal-
15 culations when the constant lidar ratio is assumed. This result is mainly due to the short integration range for the AMALi measurements, so that the assumption of the constant lidar ratio does not introduce significant error. The accuracy of the backscatter coefficient calculated with the iterative approach is assumed to be $\sigma_{bsc}^{IK}=2.0\times10^{-7}\,\mathrm{m}^{-1}\,\mathrm{sr}^{-1}$. For comparison the accuracy of the molecular backscatter
20 coefficient is $\sigma_{mol}=4.2\times10^{-8}\,\mathrm{m}^{-1}\,\mathrm{sr}^{-1}$.

The striking feature captured on backscatter ratio plots are the triangularly-shaped aerosol gradients (Fig. 8). These are related to the vertically raised isentropic surfaces and the enhanced vertical transport of sea salt aerosols. This case was studied in detail using the high resolution numerical model EULAG (Dörnbrack et al., 2009).

6 Conclusions

The robust construction and trouble-free operation over the past six years of the AMALi lidar system proved this lidar as an excellent tool for tropospheric airborne and ground based investigations for Arctic studies.

The AMALi data obtained with both standard and novel methodology approaches were successfully implemented for several case studies on various topics (Stachlewska et al., 2005, 2006c; Ritter et al., 2006; Stachlewska and Dörnbrack, 2006a; Stachlewska, 2006b; Gayet et al., 2007; Richter et al., 2008; Dörnbrack et al., 2009; Lampert et al., 2009b; Stachlewska and Ritter, 2009)

In contrast to most of the airborne evaluation approaches, requiring the difficult assessment of the backscatter coefficient calibration value along the flight in the aerosol rich lower troposphere, either by estimating it or by measuring it with additional instrumentation, the iterative calculation of the calibration value described here is precise and uses the lidar signal alone. This approach was discussed here and applied to the AMALi data. It provided the calibrated quantitative information on the particle backscatter coefficient, additionally to the qualitative range and background corrected signals provided typically by airborne lidars. The knowledge of the calibration value at any time during the flight allowed for calculations of the backscatter ratio profiles under the clear-sky conditions, obtained with the assumption of the constant lidar ratio of 20–25 sr for clear Arctic air and 30–35 sr for polluted Arctic air. These assumptions were found to be not too critical to retrieve an accurate backscatter ratio due to the short range of AMALi measurements (2.7 km) and a very stable Arctic atmosphere with quasi-uniform air mass transport. For the flights where the air mass transport had non-uniform character and the contamination with pollutants can be expected at particular altitudes, the height dependent lidar ratio should be assumed. However, the sensitivity studies performed here for both types of the retrievals showed no significant hindering, i.e. errors in the backscatter coefficient of less than $2 \times 10^{-7}\,\mathrm{m^{-1}\,sr^{-1}}$ were obtained.

References

Ansmann, A., Riebesell, M., and Weitkamp, C.: Measurements of aerosol profiles with Raman lidar, Opt. Lett., 15, 746–748, 1990. 18773

Ansmann, A., Wandinger, U., Riebesell, M., Weitkamp, C., and Michaelis, W.: Independent measurements of extinction and backscatter profiles in cirrus clouds by using a combined Raman elastic-backscatter Lidar, Appl. Opt., 31, 7113–7131, 1992. 18767, 18772

Behrendt, A. and Nakamura, T.: Calculation of the calibration constant of polarization lidar and its dependency on atmospheric temperature, Opt. Express, 10, 805–817, 2002. 18772

Dethloff, K., Rinke, A., Lehmann, R., Christensen, J.H., Botzet, M., and Machenhauer, B.: Regional climate model of the Arctic atmosphere, J. Geophys. Res., 101(D8), 23401–23422, 1996. 18746

Dörnbrack, A., Stachlewska, I. S., Ritter, C., and Neuber, R.: Aerosol distribution around Svalbard during intense easterly winds, Atmos. Chem. Phys. Discuss., 9, 16441–16481, 2009, http://www.atmos-chem-phys-discuss.net/9/16441/2009/. 18748, 18769, 18777

Ehrlich, A., Bierwirth, E., Wendisch, M., Gayet, J.-F., Mioche, G., Lampert, A., and Heintzenberg, J.: Cloud phase identification of Arctic boundary-layer clouds from airborne spectral reflection measurements: test of three approaches, Atmos. Chem. Phys., 8, 7493–7505, 2008,
http://www.atmos-chem-phys.net/8/7493/2008/. 18749

Fernald, F. G.: Analysis of atmospheric lidar observations: some comments, Appl. Opt., 23, 652–653, 1984.

Gayet, J.-F., Stachlewska, I. S., Jourdan, O., Shcherbakov, V., Schwarzenboeck, A., and Neuber, R.: Microphysical and optical properties of precipitating drizzle and ice particles obtained from alternated lidar and in situ measurements, Ann. Geophys., 25, 1487–1497, 2007,
http://www.ann-geophys.net/25/1487/2007/. 18748, 18761, 18769

Goodman, J. W.: Statistical Optics, J. Wiley & Sons, 1985. 18759

Klett, J. D.: Stable analytical inversion solution for processing lidar returns, Appl. Opt., 20, 211–220, 1981.

Klett, J. D.: Lidar inversions with variable backscatter/extinction values, Appl. Opt., 24, 211–220, 1985.

Kovalev, V. A. and Eichinger, W. E.: Elastic Lidar: Theory, Practice, and Analysis Methods, J. Wiley & Sons, ISBN 0-471-20171-5, 2004. 18773

AMALi

I. S. Stachlewska et al.

Title Page

Abstract	Introduction
Conclusions	References
Tables	Figures

|◄ | ►|

◄ | ►

Back | Close

Full Screen / Esc

Printer-friendly Version

Interactive Discussion

Lampert, A., Ehrlich, A., Dörnbrack, A., Jourdan, O., Gayet, J.-F., Mioche, G., Shcherbakov, V., Ritter, C., and Wendisch, M.: Microphysical and radiative characterization of a subvisible midlevel Arctic ice cloud by airborne observations - a case study, Atmos. Chem. Phys., 9, 2647–2661, 2009a,
http://www.atmos-chem-phys.net/9/2647/2009/. 18748, 18761

Lampert, A., Ritter, C., Hoffmann, A., Gayet, J.-F., Mioche, G., Ehrlich, A., Dörnbrack, A., Wendisch, M., and Shiobara, M.: Observations of boundary layer, mixed-phase and multi-layer Arctic clouds with different lidar systems during ASTAR 2007, Atmos. Chem. Phys. Discuss., 9, 15125–15179, 2009b,
http://www.atmos-chem-phys-discuss.net/9/15125/2009/.

Matthias, V., Böckmann, C., Freudenthaler, V., Pappalardo, G., and Bösenberg, J.: Lidar Intercomparisons on algorithm and system level in the frame of EARLINET, Hamburg, 337, ISSN 0937 1060, 2002. 18774

Richter, A., Gayet, J.-F., Mioche, G., Ehrlich, A., and Dörnbrack, A.: Mixed-Phase Clouds in the Arctic, a Synopsis of Airborne Lidar, In-Situ, and Albedometer Observations, complemented by Meteorological Analyses, in: Proceedings of 24th International Laser Radar Conference (ILRC 2008), 2, 881–884, 2008. 18748

Rinke, A., Dethloff, K., and Fortmann, M.: Regional climate effects of Arctic Haze, Geophys. Res. Lett., 31(16), L16202, doi:10.1029/2004GL020318, 2004. 18746

Ritter, C., Kirsche, A., and Neuber, R.: Tropospheric Aerosol Characterized by a Raman Lidar over Spitsbergen, in: Proceedings of 22nd International Laser Radar Conference (ILRC 2004), edited by: Pappalardo, G. and Amodeo, A., ESA SP-561, 1, 459–462, 2004. 18770

Ritter, C., Stachlewska, I. S., and Neuber, R.: Application of the two-stream evaluation for a case study of Arctic Haze over Spitsbergen, in: Proceedings of 23nd International Laser Radar Conference (ILRC 2006), edited by: Nagasawa, C. and Sugimoto, N., ISBN 4-9902916-0-3, 1, 507–510, 2006. 18770

Sasano, Y., Browell, E. V., and Ismail, S.: Error caused by using a constant extinction/backscattering ratio in the lidar solution, Appl. Opt., 24, 3929–3932, 1985.

Shimoda, K.: Introduction to Laser Physics, Springer-Verlag Berlin Heidelberg, 1986. 18762

Shipley, S. T., Tracy, D. H., Eloranta, E. W., Trauger, J. T., Sroga, J. T., Roesler, F. L., and Weinman, J. A.: A High Spectral Resolution Lidar to measure optical scattering properties of atmospheric aerosols, Part I: Instrumentation and theory, Appl. Opt., 23, 3716–3724, 1983.

AMALi

I. S. Stachlewska et al.

18773

Sicherheitstechnische Festlegungen für Lasergeräte und Anlagen, VDE-Verlag Beuth, ISSN 0178-224X, 1998. 18753

Stachlewska, I. S., Wehrle, G., Stein, B., and Neuber, R.: Airborne Mobile Aerosol Lidar for measurements of Arctic aerosols, in: Proceedings of 22nd International Laser Radar Conference (ILRC 2004), edited by: Pappalardo, G. and Amodeo, A., ESA SP-561, 1, 87–89, 2004. 18747

Stachlewska, I. S., Ritter, C., and Neuber, R.: Application of the two-stream inversion algorithm for retrieval of extinction, backscatter and lidar ratio for clean and polluted Arctic air, in: Proceedings of SPIE, 5584, 03/1–03/8, 2005. 18748, 18770

Stachlewska, I. S. and Dörnbrack, A.: Application of iterative airborne lidar inversion and its interpretation by means of ECMWF operational analyses, in: Reviewed and Revised Papers Presented at the 23rd International Laser Radar Conference (ILRC 2006), 1, 471–474, 2006a. 18748, 18769

Stachlewska, I. S.: Investigation of tropospheric arctic aerosol and mixed-phase clouds using airborne lidar technique, PhD Thesis, University of Potsdam, opus.kobv.de/ubp/volltexte/2006/698/, 2006b. 18748, 18769

Stachlewska, I. S., Gayet, J.-F., Duroure, C., Schwarzenboeck, A., Jourdan, O., Shcherbakov, V., and Neuber, R.: Observations of mixed-phase clouds using airborne lidar and in-situ instrumentation, in: Reviewed and Revised Papers Presented at the 23rd International Laser Radar Conference (ILRC 2006), 1, 325–328, 2006c. 18748, 18769

Stachlewska, I. S. and Ritter, C.: On retrieval of lidar extinction profiles using Two-Stream and Raman techniques, submitted to Atmos. Chem. Phys. Discuss., 2009. 18748, 18770

Treffeisen, R., Herber, A., Ström, J., Shiobara, M., Yamanouchi, T., Yamagata, S., Holmen, K., Kriews, M., and Schrems, O.: Interpretation of Arctic Aerosol Properties using Cluster Analysis applied to observations in the Svalbard Area, Tellus, 56B(5), 457–476, 2004. 18746

Winker, D. M., Hunt, B. H., and McGill, M. J.: Initial performance assessment of CALIOP, Geophys. Res. Lett., 34, L19803, doi:10.1029/2007GL030135, 2007. 18747

Yamanouchi, T., Treffeisen, R., Herber, A., Shiobara, M., Yamagata, S., Hara, K., Sato, K., Yabuki, M., Tomikawa, Y., Rinke, A., Neuber, R., Schumacher, R., Kriews, M., Ström, J., Schrems, O., and Gernandt, H.: Arctic Study of Tropospheric Aerosol and Radiation (ASTAR) 2000: Arctic haze case study, Tellus, 57B, 141–152, 2005. 18746

Table 1. Technical specifications of the CRF-200, Big Sky Laser, Quantel, Montana, USA.

Parameter [Unit]	Value	Comment
Maximum altitude for safe operation [m]	3000	
Beam diameter [mm]	6	
Pulse Duration [ns]	11.38	
Beam divergence [mrad] (86.5% energy)	2.59	
Pulse repetition frequency [Hz]	15	
Configuration 2003–2006		
Pulse energy at 1064 nm [mJ]	60	
Pulse energy at 532 nm [mJ]	120	
Current configuration 2006–2009		
Pulse energy at 1064 nm (residual) [mJ]]	45	absorbed by ceramic glass absorber
Pulse energy at 532 nm [mJ]	94	
Pulse energy at 355 nm [mJ]	15	

Table 2. The Maximum Permissible Exposure (MPE) values for the direct exposure of the laser radiation on the eye cornea accordingly to the Sicherheitstechnischen Festlegungen für Lasergeräte und Anlagen, VDE-Verlag Beuth 1998, ISSN 0178-224X.

Emission duration	Criterion 1 10^{-9}–10^{-7} s	Criterion 2 10^{-3}–10 s	Criterion 3 10^{-9}–10^{-7} s
Wavelength 315–400 nm	$5.6 \times 10^{3} \times t^{0.25}$ Jm^{-2}	$5.6 \times 10^{3} \times t^{0.25}$ Jm^{-2}	–
Wavelength 400–550 nm	5×10^{-3} Jm^{-2}	$18 \times t^{0.75}$ Jm^{-2}	$N^{-0.25} \times 5 \times 10^{-3}$ Jm^{-2}
Wavelength 1050–1150 nm	5×10^{-2} Jm^{-2}	$90 \times t^{0.75}$ Jm^{-2}	$N^{-0.25} \times 5 \times 10^{-2}$ Jm^{-2}

Full Screen / Esc

Table 3. Constraints on the lidar ratio dependent on the air type. Corresponding errors of the backscatter coefficient calculation are given.

Arctic air type	clean	low aerosol load	considerable aerosol load	polluted
B(h)=const [sr]	20	25	30	35
$\Delta\beta_{t1}^{part}$ [m^{-1}sr^{-1}]	$\pm1.8\times10^{-7}$	$\pm0.3\times10^{-7}$	$\pm0.7\times10^{-7}$	$\pm1.4\times10^{-7}$

AMALi

I. S. Stachlewska et al.
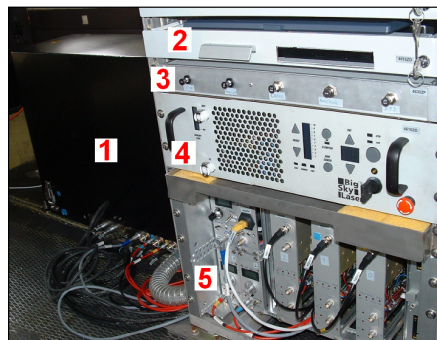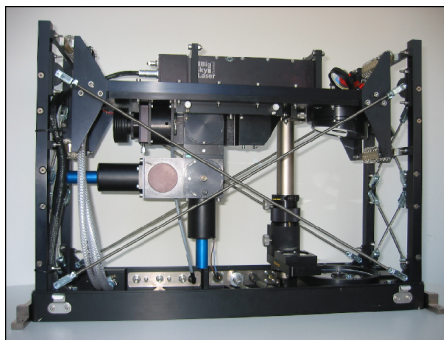
Fig. 1. The AMALi in a nadir-aiming airborne configuration on board the Polar 2 aircraft (right) and the optical assembly (left). The main elements are the optical assembly (1), laptop (2), safety breaker box (3), laser control and cooling unit (4), and transient recorders (5).

Fig. 2. The AMALi in a zenith-aiming airborne configuration on board the Polar 2 aircraft (left) and the Polar 5 aircraft (right).
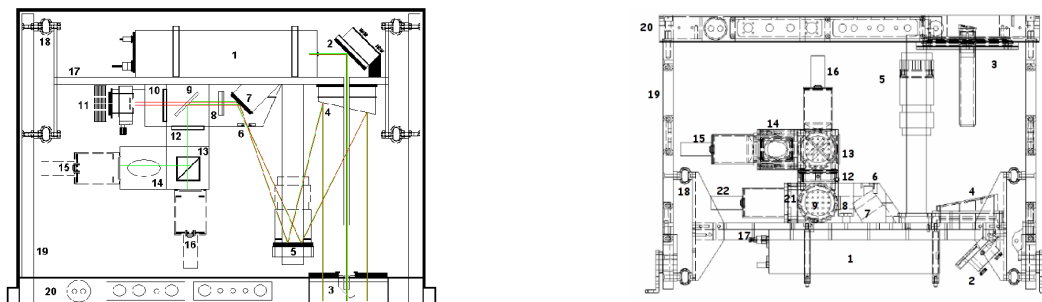
Fig. 3. The AMALi optical assembly with schematically drawn ray-tracking at 532 nm (green) and 1064 nm (red) is given on the left drawing (configuration 2003–2006, nadir). The numbers indicate the main components in the assembly; 1. laser head 2. directing mirror in piezo motor 3. window with Brewster's angle 4. off-axis parabolic mirror 5. first folding mirror 6. pinhole 7. second folding mirror 8. achromatic lens 9. beam splitter 10. interference filter for 1064 nm channel 11. APD for 1064 nm detection 12. interference filter for 532 nm channel 13. polarizing cube 14. thin film polarizing filter 15. PMT for perpendicular 532 nm detection 16. PMT for parallel 532 nm detection 17. optical bench 18. springs 19. posts 20. base plate. The drawing on the right depicts the present configuration (zenith pointing) were the IR detection channel is replaced with the UV channel (21. interference filter for 355 nm channel and 22. PMT for perpendicular 355 nm detection).
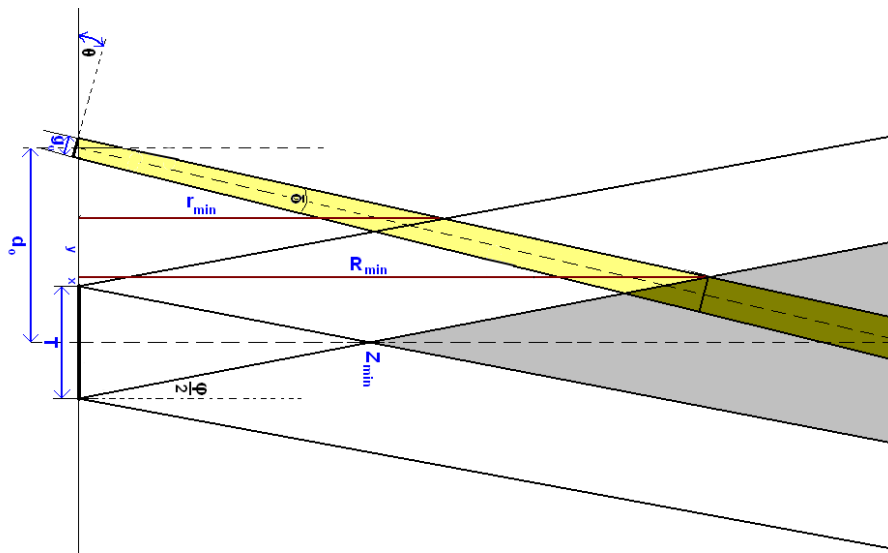
Fig. 4. The overlap between the emitted laser beam and the field of view of the telescope.

AMALi

I. S. Stachlewska et al.

Printer-friendly Version
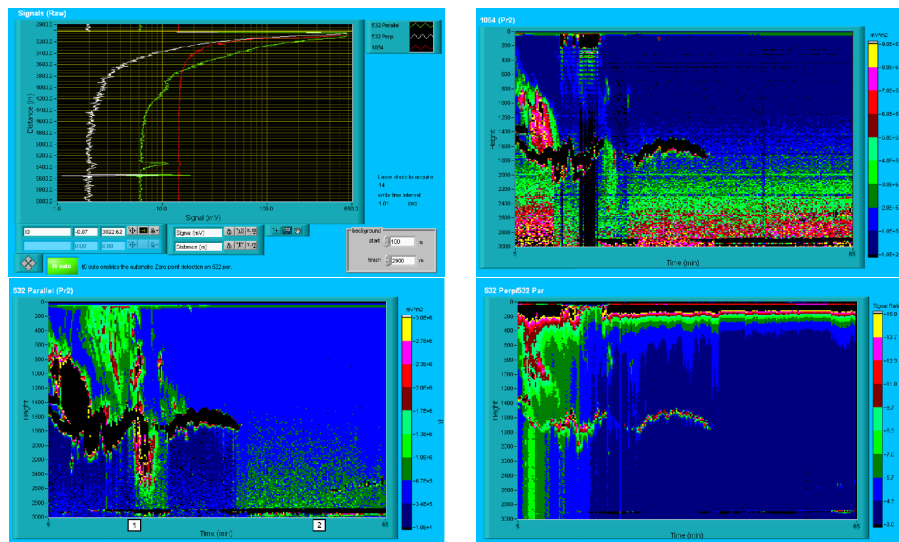
Interactive Discussion

Fig. 5. The quick-look displays of the AMALi on-line software for the nadir-aiming configuration on board the Polar 2 aircraft providing the signal evolution in a real-time during the flight. Display of the raw signals at 532 nm, 532 nm perp. and 1064 nm (left top), the range and background corrected signals at 532 nm (left bottom) and 1064 nm (right top), and the depolarization ratio at 532 nm (right bottom). Evidence of mixed-phase clouds and precipitation.

AMALi

I. S. Stachlewska et al.
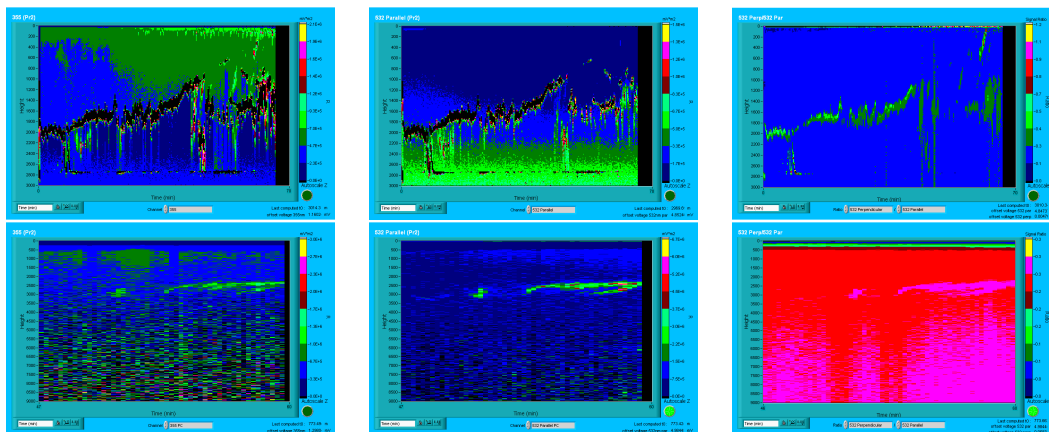
Fig. 6. The quick-look displays of the AMALi on-line software for the nadir-aiming (top figures) and zenith-aiming (bottom figures) configuration on board the Polar 2 aircraft. The display of the range and background corrected signals evolution at 355 nm, 532 nm and the depolarization ratio at 532 nm is provided in a real-time during the flight. Top: precipitating mixed-phase clouds, and bottom: ice cloud at 3 km.
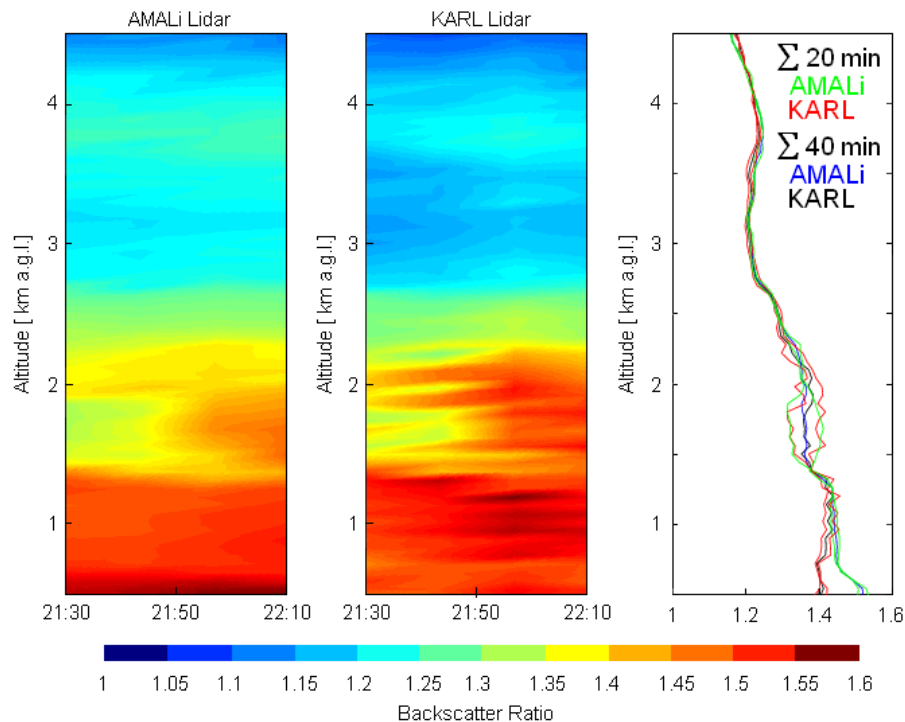
Fig. 7. The comparison of the 532 nm backscatter ratio profiles retrieved from measurements between 21:30–22:10 UT on 15 June 2004 for AMALi and KARL lidars. Both lidars operated in a zenith-looking ground based configuration. Subvisible clouds passing above the lidar site between 1.5–1.8 km are captured.

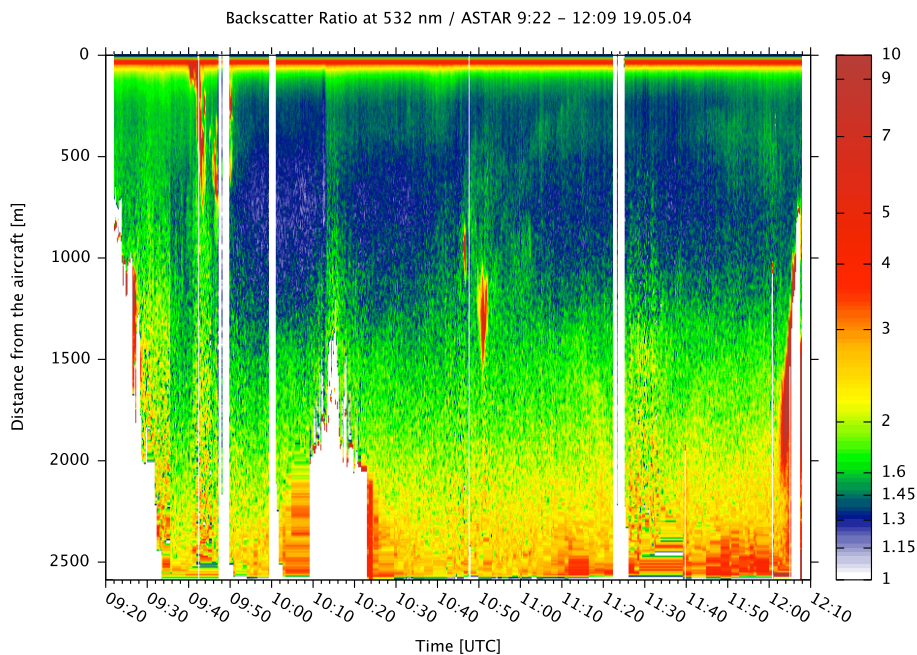Backscatter Ratio at 532 nm / ASTAR 9:22 – 12:09 19.05.04

Fig. 8. The calibrated backscatter ratio profiles along the flight retrieved using the iterative approach for 19 May 2004. The data were obtained by the nadir-aiming airborne AMALi lidar from the flight altitude of 2650 m during the ASTAR 2004 campaign.